

pubs.acs.org/JPCB Article

Energy Transport in Class B GPCRs: Role of Protein—Water Dynamics and Activation

Humanath Poudel and David M. Leitner*



Cite This: J. Phys. Chem. B 2022, 126, 8362-8373



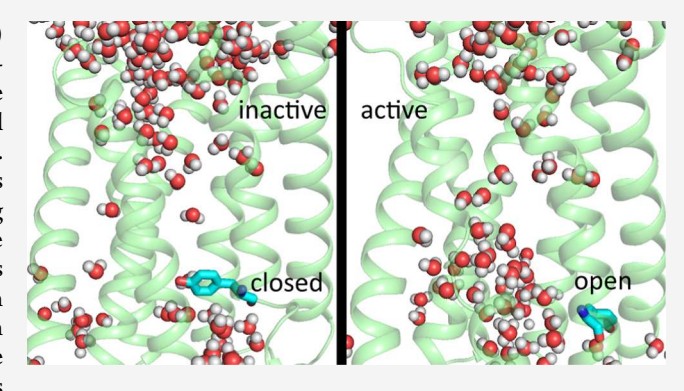
ACCESS

III Metrics & More

Article Recommendations

Supporting Information

ABSTRACT: We compute energy exchange networks (EENs) through glucagon-like peptide-1 receptor (GLP-1R), a class B G-protein-coupled receptor (GPCR), in inactive and two active states, one activated by a peptide ligand and the other by a small molecule agonist, from results of molecular dynamics simulations. The reorganized network upon activation contains contributions from structural as well as from dynamic changes and corresponding entropic contributions to the free energy of activation, which are estimated in terms of the change in rates of energy transfer across non-covalent contacts. The role of water in the EENs and in activation of GLP-1R is also investigated. The dynamics of water in contact with the central polar network of the transmembrane region is found to be significantly slower for both activated states



compared to the inactive state. This result is consistent with the contribution of water molecules to activation of GLP-1R previously suggested and resembles water dynamics in parts of the transmembrane region found in earlier studies of rhodopsin-like GPCRs.

1. INTRODUCTION

Both structural and dynamic changes that occur with ligand binding contribute to allosteric regulation of G-proteincoupled receptors (GPCRs), as exemplified by the role of microswitches and transmembrane water in activation. While class A rhodopsin-like GPCRs have been studied for some time, structures for class B GPCRs have only become more recently known,⁸⁻¹⁷ allowing further studies probing how they function, including molecular dynamics (MD) simulations, which are already beginning to examine structural and thermodynamic properties.¹⁸ While all GPCRs contain seven transmembrane helices, class B GPCRs have distinct motifs from their class A counterparts, regions with conserved residues many of which undergo structural change during activation. The dynamics of transmembrane water in class B GPCRs has not yet been studied for both inactive and active states, in contrast to the detailed information that has been learned through investigations of water in class A receptors. 4,6,19-22 Further information about how class B GPCRs respond to ligand binding would be useful, including the role of dynamic and corresponding entropic changes during activation. Here, we report the results of MD simulations to characterize the dynamics of transmembrane water molecules in the inactive and two active states, each with a different ligand, one a peptide ligand and the other a small molecule agonist, of the class B glucagon-like peptide 1 receptor (GLP-1R). We examine the transport of vibrational energy through the receptor in the three states and the role of water in that process. We identify both structural and dynamic contributions

to energy transport and estimate changes in entropy with activation in terms of corresponding changes in rates of energy transfer across non-covalent contacts.

GLP-1R regulates blood glucose control, bone turnover, and cardiovascular development.²³ It is a potential drug target of type 2 diabetes, psychiatric disorders, neurodegeneration, and cardiovascular diseases.²⁴ Several forms of GLP-1, a peptide ligand, and various other endogenous agonists activate GLP-1R, and are either under development or approved for the treatment of type 2 diabetes. 24,25 However, due to the route of administration and their side-effect profile, peptide drugs may not be optimal, and currently, efforts are being taken to develop non-peptide drugs, which can be orally administered and have reduced side effects, but understanding their activation mechanisms remains a challenge.²⁶ Recent reports of crystal structures of GLP-1R²⁷ provide the possibility of studying these systems by MD simulations. Here, we present an MD simulation study of GLP-1R in two active states, one bound with a peptide ligand and the other with a non-peptide agonist, and one inactive state. We compute rates of energy transfer across non-covalent contacts, which are related to

Received: June 7, 2022 Revised: October 3, 2022 Published: October 18, 2022





changes in both the structure and dynamics of the receptor upon activation.

Crystal structures reveal the presence of transmembrane water (TW) for class A, rhodopsin-like GPCRs. ^{4,6,19,21,22} For class B GPCRs, some studies indicate the presence of TW forming polar interactions with transmembrane residues, ^{16,27} though crystal structures have not yet provided a detailed picture of the functional role of water. In the MD simulations carried out here, time is permitted for water from outside and inside the cell to enter the transmembrane region and some of the TW dynamics subsequently studied. The relaxation dynamics of water—protein hydrogen bonds around the central polar network, previously identified as an important region of polar network formation between residues and water, ¹² is investigated. We also identify the location, gating, and mobility of water in different regions and pockets of GLP-1R.

Energy transport in proteins is anisotropic and is mediated by both protein structure and dynamics. 28–40 The rate of energy transfer across non-covalent contacts depends on the dynamics of the contact, as we discuss below, so that there is a change in the rate of energy transfer across the contact that corresponds to changes in dynamics and change in entropy, with change in the functional state of the protein. Energy transfer in GLP-1R is studied by computing energy exchange networks (EENs), which have been computed for several allosteric proteins in the past, 41 including the β_2 -adrenergic receptor, a rhodopsin-like GPCR.⁴² We adopt the computational tools developed by Yamato and coworkers 43,44 for the computation of EENs from the results of MD simulations for the inactive and two active states of GLP-1R. Contributions of changes in structure and dynamics to the EENs upon activation are analyzed and used to provide estimates to changes in entropy in terms of change in rates of energy transport across non-covalent contacts that occur when GLP-1R is activated. The role of water in this process is also addressed.

In the following section, we summarize the computational methods used for the study of energy transport, structural, and water dynamics of GLP-1R. In Section 3, we present results for the energy transport properties (Section 3.1), their connection to structural dynamics and entropy (Section 3.2), and TW dynamics (Section 3.3). Concluding remarks are given in Section 4.

2. COMPUTATIONAL METHODS

We studied the inactive state of GFP-1R and two active states, one with bound peptide GLP1 and one activated by a small molecule, FFR. We refer to the former as the GLP1-active state [protein data bank (PDB) 5VAI¹³] and the latter as the FFRactive state (PDB 7C2E¹⁷). Coordinates of the inactive state were taken from PDB 6LN2.10 Missing residues connecting transmembrane helix 1 (TM1) to the extracellular domain (ECD) in all states were modeled using Modeller9.23,45 as were the missing residues of intracellular loop (ICL) 2 of the inactive state. This ICL, added to purify the protein, was removed in the inactive state. For the FFR-active state, ICL 3 was modeled using Modeller9.23.45 With these modifications, all states contain the same homology of 393 amino acid sequences for consistency. The forcefield parameters of FFR were generated using the CHARMM General Force Field (CGenFF) interface of the CHARMM-GUI.⁴⁶ Initial conditions for all states were set up using the CHARMM-GUI⁴⁶ online interface in a rectangular box embedded with 170 1palmitoyl-2-oleoyl-sn-glycero-3-phosphocholine lipid molecules and about 21,000 water molecules. Neutralization was performed using Na⁺ and Cl⁻ ions with a final concentration of 0.15 M NaCl. All simulations were performed with the AMBER20 MD software package using the TIP3P model for waters, the Lipid17⁴⁷ force field for lipids, and the AMBER ff14SB⁴⁸ force field for the protein.

For the simulations, minimization was done with 20,000 steps using the steepest descent method for the first 10,000 steps and conjugate gradient method for the remaining. Periodic boundary conditions were applied. A heating NVT simulation was carried out starting from 0.1 to 300 K for 1 ns and continued an additional 1 ns at 300 K with the Berendsen thermostat.⁴⁹ Positional restraints with a force constant of 1 kcal/(mol·Å²) were applied to backbone atoms and all hydrogen-containing bonds were constrained with the SHAKE algorithm. ⁵⁰ Equilibration was done for 10 ns with position restraints on protein backbone atoms with a force constant of 1 kcal/(mol·Å²), followed by another 20 ns without restraints. To allow water to penetrate into the transmembrane region, we performed 600 ns NPT simulations, sufficient for the number of TW to remain fairly constant. This was examined via water counts, discussed below, and the RMSD convergence of the proteins (see Supporting Information). Trajectory files were saved each ns for subsequent NVE simulations.

To identify signaling pathways, energy currents were computed between residues and residue-water pairs by selecting a trajectory every 2 ns from the 500 to 600 ns NPT simulations. Each NVE simulation was allowed to evolve for 150 ps, with an integration time of 0.5 fs. Coordinates and velocities were saved every 5 and 1 fs, respectively. An Ewald sum tolerance of 10⁻⁷ was selected to reduce energy drift. EENs were computed using the CURrent calculation for proteins (CURP) version 1.2.1 developed by Yamato and coworkers. 43 Briefly, the EEN is constructed as follows: starting with the interatomic energy flux, 43,51 $J_{i \leftarrow j}^{k} = \frac{1}{2} (\mathbf{v}_{i} \bullet \mathbf{F}_{ij} - \mathbf{v}_{j} \bullet \mathbf{F}_{ji})$, where $J_{i \leftarrow j}^{k}$ is the inter-residue atom-atom energy flow between atoms i and j for trajectory k, ν is the velocity and F is the force of one atom on the other, and the inter-residue energy flux is 43 $J_{A \leftarrow B}^k(t) = \sum_{i \in A}^{N_A} \sum_{j \in B}^{N_B} J_{i \leftarrow j}^k(t)$, where N_A (N_B) is the number of atoms in residue $\stackrel{.}{A}$ (B). Energy currents, L_{AB} , are computed by averaging $L_{AB}^k = \frac{1}{RT} \lim_{\tau \to \infty} \int_0^{\tau} \langle J_{A \leftarrow B}^k(t_0) J_{A \leftarrow B}^k(t+t_0) \rangle dt$, where R is the gas constant and T is the temperature. L_{AB} is multiplied by RT and values reported in $(kcal mol^{-1})^2 ps^{-1}$, yielding G_{AB} , where $G_{AB} = (RT)L_{AB}$, referred to as energy conductivity. We drop subscripts AB in the following. An autocorrelation function window of 25 ps was chosen to evaluate G. For the CURP calculation, we only included TWs remaining near a residue at least 50% of the NVE simulation time. Contacts were identified between atoms of residues and oxygen of TWs within 3 Å. All stable TWs were evaluated as a single water cluster for the calculation of G. On average, there are a total of 37.5 TWs in the inactive state, 39.3 for the GLP1active state, and 38.7 for the FFR-active state.

In total, 50 CURP calculations were performed for each state of GLP-1R. We average the results to evaluate the EENs, as well as the difference in energy exchange networks, Δ EEN, and relative difference in energy exchange networks ($r\Delta$ EEN) upon activation. The Δ EEN was computed by subtracting the

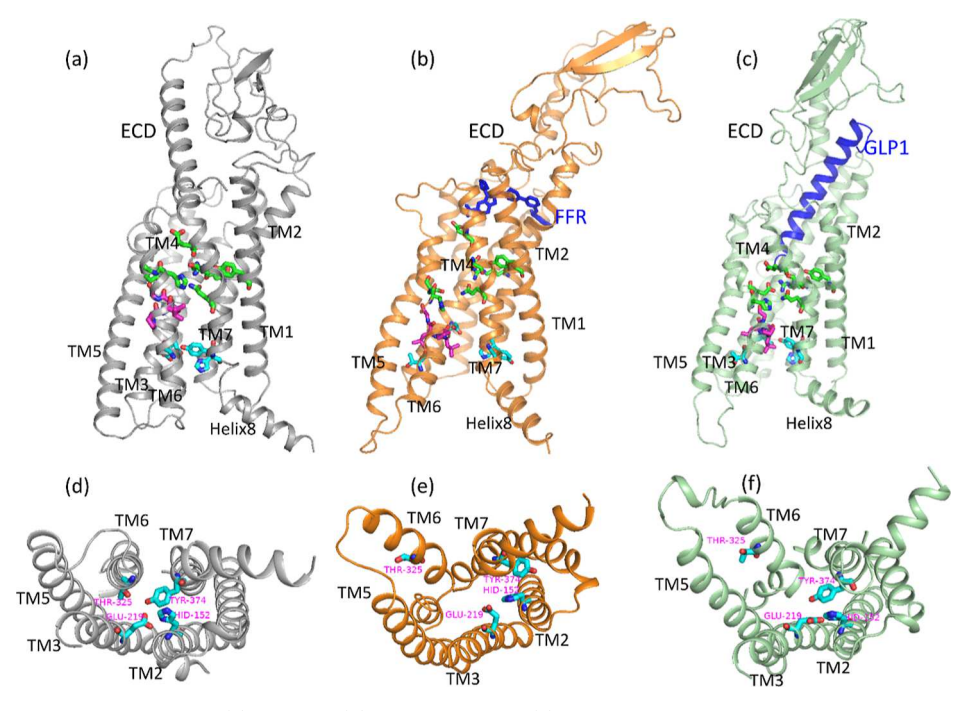


Figure 1. Top row: side view of GLP-1R in (a) inactive, (b) FFR-active, and (c) GLP1-active states. The ligands are colored blue. The snapshots are taken from the simulations at 600 ns. The central polar network is shown as green sticks, the PxxG (Pro-x-x-Gly) motif in sticks with magenta, and the HETx (His-Glu-Thr-x) in cyan. Bottom: cytoplasmic view of the GLP-1R and the HETx motif, illustrating the change in polar networks in the motifs with activation, is shown in the (d) inactive, (e) FFR-active, and (f) GLP1-active states. Transmembrane helices are labeled.

average G of the inactive state from each active state. The relative difference⁴² was computed as $r\Delta \text{EEN} = \frac{G_{\text{active}} - G_{\text{inactive}}}{G_{\text{active}} + G_{\text{inactive}}}$, where G_{active} and G_{inactive} correspond to the average G values for contacts of active and inactive states, respectively. To evaluate $r\Delta \text{EEN}$, a threshold of $G > 10(\text{kcal mol}^{-1})^2$ ps⁻¹ was selected.

We examine the relation between G and equilibrium fluctuations in the length of non-covalent contacts of GLP-1R, from which we can relate changes in G to changes in dynamics of the contact and entropy associated with the dynamics. It has been argued for a non-covalent contact in the harmonic approximation that G is proportional to $\langle \delta r^2 \rangle^{-1}$,^{38,52,53} and this proportionality has been found to hold well for polar contacts of proteins based on the results of MD simulations. 35,52-55 If a contact remains intact, change in dynamics of the contact with change in state of the protein can lead to a change in G. Thus, if the rate of energy transfer across a contact, proportional to G, is measured in the inactive state and in the active state, a change can be associated with a change in dynamics of the contact and associated entropy. Below we plot G versus $\langle \delta r^2 \rangle^{-1}$ for several contacts that remain largely intact during activation to examine if they are proportional. It is helpful when visualizing the data to average *G* in intervals of $\langle \delta r^2 \rangle^{-1}$, and we therefore also bin the data. For polar contacts, we use bin sizes of 412.41 nm⁻²; for hydrogen bonds between charged groups formed by Tyr117-Asp170 and Arg199-Asp265, we use 357.17 nm⁻²; and for contacts formed by Asp194-Arg199 and Asp36-Arg46, we use of 244.41 nm⁻². In all cases, we examine proportionality with linear fits to all the data as well as to the binned data.

If G_1 and G_2 are proportional to the rate of energy transfer across a non-covalent contact of the inactive and active state, respectively, then in the harmonic approximation, using the proportionality between G and $(\delta r^2)^{-1}$, the change in entropy

upon activation associated with a change in the dynamics of the contact is given by 52,53

$$\Delta S = \frac{k_{\rm B}}{2} \ln \left(\frac{G_1}{G_2} \right) \tag{1}$$

If the rate of vibrational energy transfer across the contact can be measured before and after activation, changes in entropy associated with the dynamics of that contact can be estimated. S2,53 It is assumed in eq 1 that a contact remains unbroken during activation, though in practice contacts break and reform. We include in our analysis only contacts that remain intact at least 50% of the simulation time in both states. Then, if f_a is the fraction of time and the contact is intact in the active state, we take G_2 to be G computed for the residue pair in the active state divided by f_a , thus assuming that during the time, the contact is broken and the value of G for the residue pair can be neglected. We do the same for the inactive state to obtain G_1 .

The non-covalent contacts are categorized as polar and charged. Polar contacts are AH···O, where A is oxygen or nitrogen and the H···O distance is no greater than 2.8 Å. An angle AHO $\geq 150^\circ$ was selected for hydrogen bonds, a subclass of polar contacts. A polar contact is analyzed only if it remains intact 99% of the time that a value of *G* is computed. For the length of a polar contact, *r*, the variance is $\langle \delta r^2 \rangle = \langle (r - \langle r \rangle)^2 \rangle$ and is computed and paired with the respective *G*. Contacts with $-{\rm NH_3}^+$ and COO $^-$ are classified as charged. We introduced a threshold of $\Delta G > 50$ (kcal mol $^{-1}$) 2 ps $^{-1}$ for $\Delta \rm EENs$.

For analysis of water dynamics, we first count the number of TW for all states of GLP-1R. Hydrogen bond correlation functions were computed for protein-water interactions, defined as $C_{\rm HB}(t) = \langle h(t)h(0)\rangle/\langle h(0)\rangle$ where 0 is the initial time and h(t) is 1 if a hydrogen bond exists at time t, even if it

was broken between 0 and t, otherwise it is 0. The analysis was made in the 500-600 ns interval of the simulation.

3. RESULTS AND DISCUSSION

We begin with energy transport in GFP-1R, then turn to activation-induced changes in energy transport and entropy, and finally present results for transmembrane water (TW) dynamics. Each property studied is connected to the structure of GLP-1R. Structures of GLP-1R in the inactive, GFP1-active, and FFR-active states taken from the end of the simulations are shown in Figure 1. GLP-1R has an extracellular domain (ECD) consisting of the first 110 residues, a transmembrane region with seven transmembrane helices (TM) each connected by either an extracellular or intracellular loop, and one remaining helix (helix 8) mainly in the intracellular region. The ECD appears closed in the inactive state bending toward the TM helices and open in the active state to accommodate ligands. The central polar network consists of residues below the ligand-binding pocket, facilitates signaling from the ligand to the cytoplasmic side, and includes interactions with TW. Motifs containing conserved class B GPCR residues are indicated. The Pro-x-x-Gly (PxxG) motif is in the middle of TM6. PxxG helps shift the lower half of TM6 upon activation by forming a kink. The His-Glu-Thr-x (HETx) motif facilitates opening the cytoplasmic site in the activation process by breaking polar networks, thereby shifting TM6 outward and accommodating the G-protein in the cytoplasmic region. Tyr374 plays a key role in water gating inside the TM region, discussed below.

3.1. Energy Exchange Networks. To explore the energy dynamics in the inactive and active states of GLP1-1R, we computed EENs, which reveal regions through which energy flow in the different states of this protein is facile. ⁴³ Complete EENs are presented in Figure S1, which includes values of *G* between residue pairs and between residues and TWs. The residues involved in contacts contributing significantly to the EENs are shown in Figure 2. Most of these contacts include TM2, TM3, TM4, TM6, and TM7 and some in the ECD. There are notable differences in the EENs between inactive and active states in the region spanning the ECD and the TM helices. The orientation of the ECD shifts with activation, thereby affecting interactions and the EENs. In the TM region,

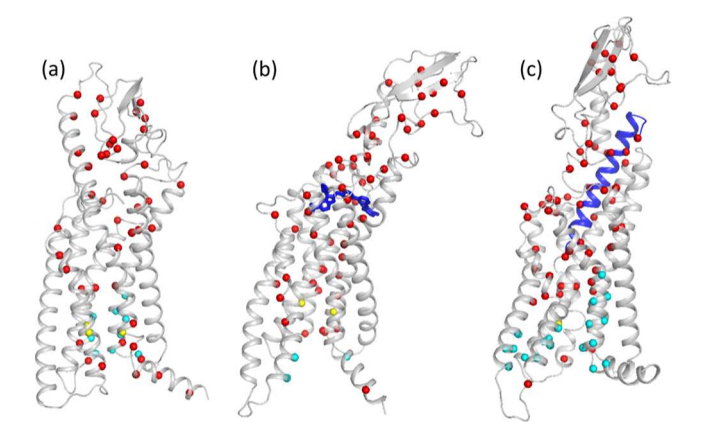


Figure 2. Residues forming contacts that contribute to the EENs of GLP-1R for (a) inactive, (b) FFR-active, and (c) GLP1-active states are shown, where the ligands are colored blue. For the residue-TW contacts, the residues are colored cyan. Residues that belong to motifs are indicated in yellow.

notable differences involve some residue-TW interactions. The inactive state and the GLP1-active state have more contact with water than the FFR-active state, which will be further discussed below.

We find that water can play an important role in energy transfer between residues of the TM region, which we refer to as a water bridge. All contacts contributing to water bridges are listed in Tables S2–S4 and shown in Figure S8. To define a water bridge as residue-TW-residue, we first calculated the native contact formation between water with both residues. Several significant water bridges are found to contribute to the EENs. For example, for the inactive state (see Table S2A,B), Ala157-TW and TW-Trp246 have *G* of 61.3 and 39.37 (kcal mol⁻¹)² ps⁻¹, respectively, as compared to a *G* for the contact without water, Ala157-Trp246, of only 2.48 (kcal mol⁻¹)² ps⁻¹. Overall, water bridges are observed (Figure S8) primarily for contacts between TM2, TM3, TM6, and TM7.

We consider changes to the EEN due to activation, Δ EEN, which we define as the difference between the EEN for the active and inactive states. To obtain the Δ EENs, we subtract all residue—residue and residue-TW values of *G* for the inactive state from one of the two active states. We plot ΔEEN for the FFR-active state in Figure 3a and the GLP1-active state in Figure 3b. The locations of contacts making the largest contributions to the $\Delta EENs$ are shown in Figure 4a,b for FFRactive state and GLP1-active state, respectively. We note that we do not include in Figure 4 the large differences appearing near the diagonal in Figure 3, which correspond to energy transfer along the main chain. Rates of energy transfer along the main chain are relatively large and their differences can appear large on the scale used in Figure 3. We also point out the data plotted in Figure 3 could be further analyzed to identify regions where energy transport pathways change during activation, as done for the β_2 adrenergic receptor.⁴ Here, we focus on how differences in dynamics of specific noncovalent contacts in the different states, as well as structure, contribute to the Δ EENs. The full list of contacts seen in both Δ EENs is listed in Table S5.

There are several notable similarities between the $\Delta EENs$ of GLP1-active and FFR-active states. Both $\Delta EENs$ show effects of the opening of TM6 away from TM3 and TM4, which opens the GPCR in the cytoplasmic region for G-protein binding. The breaking of polar interactions between the residues of the HETx motif is seen, notably Glu219-Thr325. Pro330-Thr334, where Pro330 belongs to the PxxG motif, also contributes to a negative ΔEEN in both active states as Pro330 moves away from Thr334, while the TM6 forms a sharp kink during activation and moves outward. These contributions to the $\Delta EENs$ are related to structural changes.

We also find differences in the two $\Delta EENs$, most notably in the ECD, in which the orientation of ECD is different in each state. The interaction with water is also different in the two $\Delta EENs$. The FFR-active state has fewer residue-TW contacts than the GLP1-active state. In the GLP1-active state, water interacts with residues of TM5, TM6, and TM7. The GLP1-active state is characterized by many contacts in TM7, including residues of the central polar network.

The $\Delta EENs$ presented here capture some features of another class B GPCR recently studied by MD simulations. The activation mechanism of the glucagon receptor GCGR, a prototype class B GPCR and, like GLP-1R, a member of the B1 subfamily, was studied by evaluating the results of MD simulations and the conformational free energy landscape. ¹⁸

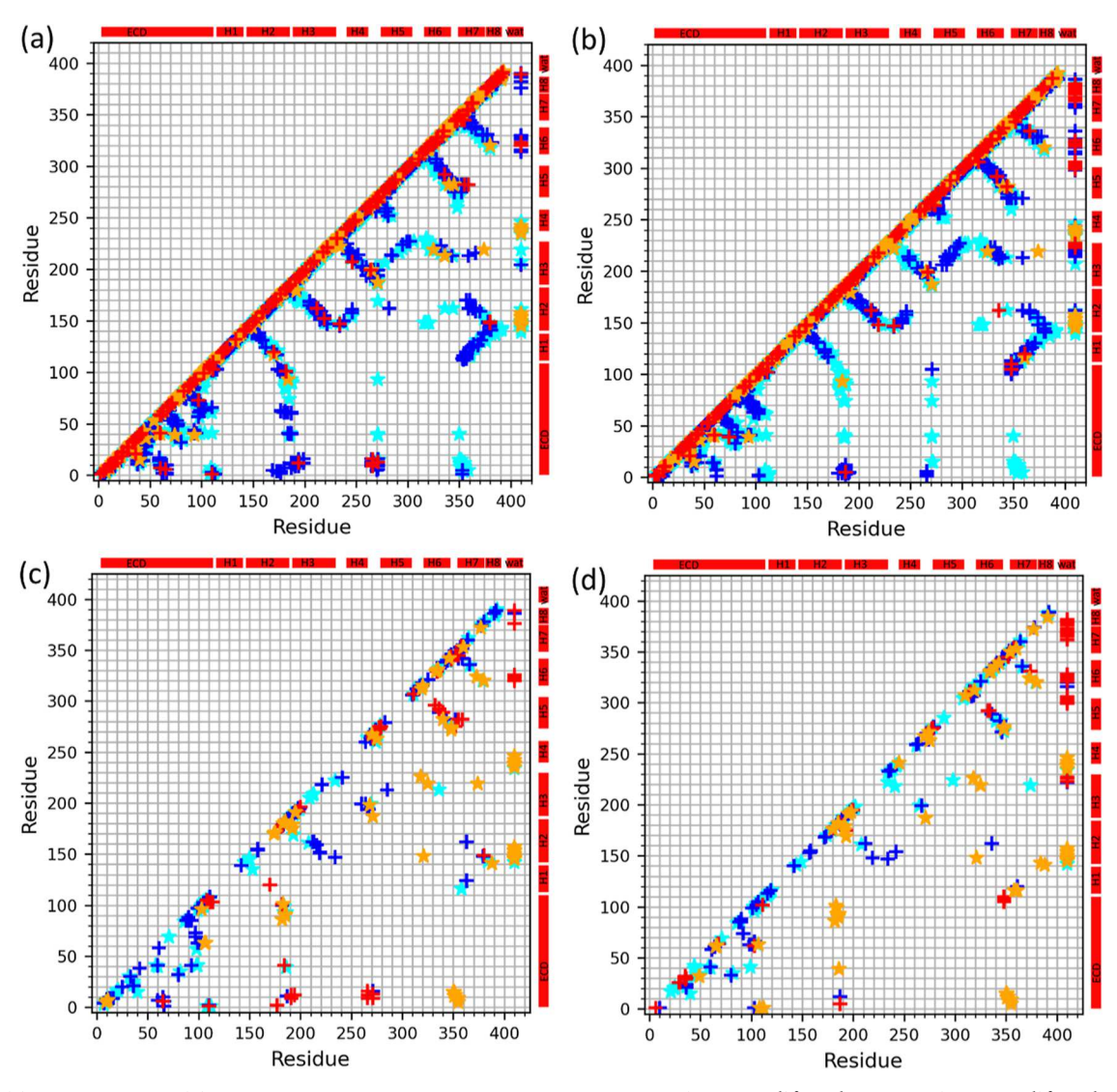


Figure 3. (a) FFR-active and (b) GLP1-active ΔEEN. The ΔG values for blue 2–50 (kcal mol⁻¹)² ps⁻¹, red >50 (kcal mol⁻¹)² ps⁻¹, cyan –2 to –50 (kcal mol⁻¹)² ps⁻¹, and orange <-50 (kcal mol⁻¹)² ps⁻¹. (c) FFR-active and (d) GLP1-active $r\Delta$ EEN. Blue (\star) corresponds to 0.7–0.9, red (\star) >0.9, cyan (+) –0.9 to –0.7, and orange (+) <-0.9. Transmembrane helices and extracellular domain, ECD, are labeled in the sidebar. Transmembrane water-residue values appear in the rightmost column.

The energy landscape reveals three states, where the inactive is lowest in free energy, while partial and fully active states are higher. The free energy change was represented in terms of the distance between TM6-TM3 and the angle of rotation of the residues of the PxxG (Pro330-Leu331-Leu332-Gly333) motif, which creates a pocket to the G-protein to bind in the cytoplasmic region. Class B GPCR activation is generally stabilized by the rearrangements of the motif residues and polar networks. In our study of GLP-1R, the polar interaction of Pro330 from PxxG with Thr334 breaks upon activation and helps to shift TM6 outward, yielding a large negative change in the $\Delta EENs$.

Another notable feature found in the computational study of GCGR is that the polar interactions in the HETx (His152-Glu219-Thr325-Tyr374) motif break upon activation and rearrange for further stability. In GLP-1R, the contacts Glu219-Thr325 and Glu219-Tyr374 of the HETx motif break, yielding negative changes in both Δ EENs. Similarly, contacts between Glu219 of the same motif and residues of TM2 yield positive Δ EENs, specifically formation of Glu219-His152 in

the GLP1-active state and Glu219-Arg148 in the FFR-active state.

While Δ EENs reveal both structural and dynamic changes upon activation, they can miss contributions of van der Waals contacts, for which the absolute values of G are often small and so their difference is small. However, the relative change upon activation, which we refer to as $r\Delta EEN$, may not be small.⁴² Contacts that make the largest contribution to $r\Delta EEN$ are shown in Figure 3c for activation by FFR and 3d for activation by GLP1. In Figure 4c, we find a larger number of motif residues than for the Δ EEN plotted in Figure 4a, in particular, the appearance of residues of the PxxG motif. Contacts of the $r\Delta$ EEN form a more continuous network from the ligand to TM5 and ultimately the cytoplasm compared to the Δ EEN. Similarly, for the $r\Delta EEN$ corresponding to transition to the GLP1-active state, we observe five motif residues, one more than we found for the corresponding ΔEEN and the $r\Delta EEN$ exhibits a more continuous pathway for energy transfer from the peptide ligand via TM7 to the cytoplasm. As found for the β_2 -adrenergic receptor, ⁴² the $r\Delta$ EEN appears to encompass

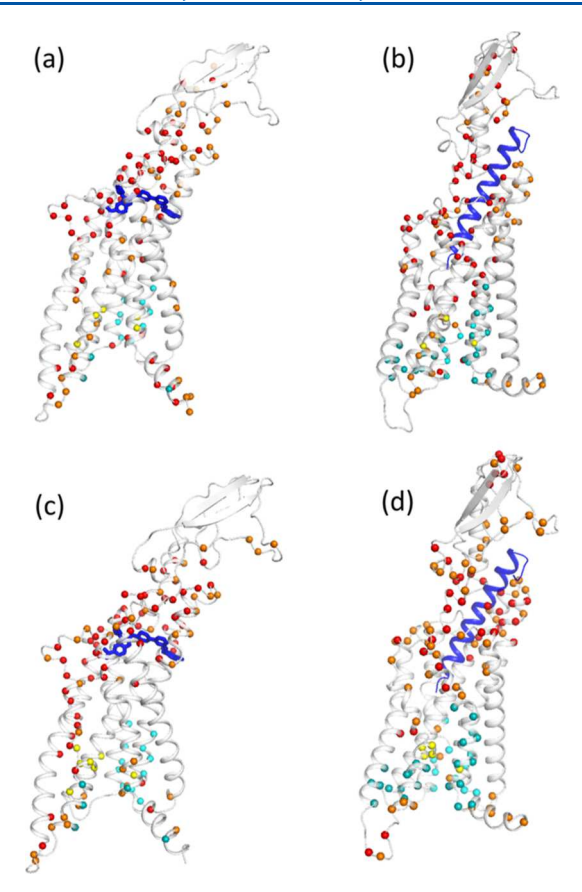


Figure 4. (a) FFR-active and (b) GLP1-active ΔΕΕΝ. Residue—residue contacts and residue-TW contacts where $\Delta G > 50$ (kcal mol⁻¹)² ps⁻¹ are red and dark cyan, respectively; residue—residue contacts and residue-TW contacts where $\Delta G < -50$ (kcal mol⁻¹)² ps⁻¹ are orange and cyan, respectively. Yellow indicates the residues in PxxG and HETx motifs. (c) FFR-active and (d) GLP1-active $r\Delta$ EEN. Residue—residue contacts and residue-TW contacts where the ratio is larger than 0.9 are red and dark cyan, respectively; residue—residue contacts and residue-TW contacts where the ratio is less than -0.9 are orange and cyan, respectively. Yellow indicates the residues in PxxG and HETx motifs.

more motif residues involved in activation than the ΔEEN and reveals a more continuous pathway from the ligand-binding region to the cytoplasm.

Some of the changes seen in $\Delta EENs$ can be related to change in the structure found in contact or distance maps. In past studies, we have examined correlations between interresidue distance and rates of energy transfer between residues, where we have found some correlation but also large variations in the rate for a given distance. For GLP-1R, we have computed maps of distances between residues from the structures sampled over the final 100 ns of the simulation. Distance maps are plotted in Figure S2 for the inactive, FFR-active, and GLP1-active states. Changes in the distance map, Δd (active—inactive), are plotted in Figure S3 for FFR-active for GLP1-active states. These maps are differences in center of mass distances between residue pairs plotted in Figure S2.

Overall, larger distances upon activation are found for TM3-TM6 and TM6-TM7, whereas TM6 is seen to move toward TM5, trends that underlie some of the changes seen in the EENs in Figure 3. However, we also find notable differences when comparing the Δd map to the ΔEEN map. ΔEEN can be sizeable where there is no noticeable change in distance. We

will discuss below sizable contributions to ΔEEN where we find Δd to be small (in almost all cases under 0.5 Å and in two cases up to 1.3 Å). The origin of the contribution to the change in the rate of energy transfer across a contact, the length of which changes little upon activation, is dynamic, as discussed below.

3.2. Change in EENs and Change in Entropy upon Activation. The Δ EEN results from a combination of structural and dynamic changes. The latter represent dynamical contributions to allostery, which have been the focus of much attention, $^{61-69}$ and we examine them for the activation of GLP-1R. For many non-covalent contacts, G has been found to be proportional to the inverse of the variance in the length of the contact, that is, $G \propto \langle \delta r^2 \rangle^{-1.35,52-55}$ To determine changes in dynamics and corresponding changes in entropy associated with the Δ EEN for activation of GLP-1R, we first examine G and the corresponding dynamics of the contact.

To investigate dynamic contributions to the ΔEEN , as opposed to structural, we computed the fraction of time the contacts of each ΔEEN remain intact during the full 100 ns simulation data we sampled for the calculation. In particular, we identified contacts that remain intact at least 50% the full simulation time used to compute the $\Delta EENs$ and checked that the dynamical changes of the contact made the larger contribution to the change in G upon activation. For such hydrogen-bonded contacts making sizable contributions to the $\Delta EENs$ [at least 50 (kcal mol⁻¹)² ps⁻¹], we identified seven that remained intact from the inactive to the FFR-active state and five from the inactive to the GLP1-active state. The contacts are spread around different regions of the protein, as shown in Figure S6.

We begin with polar contacts of all three states of GLP-1R that meet the criteria as described above. For GLP-1R, these polar contacts are Cys18-Leu22, Ala322-Leu326, Tyr207-Trp246, Ile317-Leu321, Glu359-Thr363, and Ser324-Leu328. The complete data for these contacts are shown in Figure S4. For clarity we bin the data, as detailed in Section 2, and plot the results in Figure 5. The data appear to fall along the same

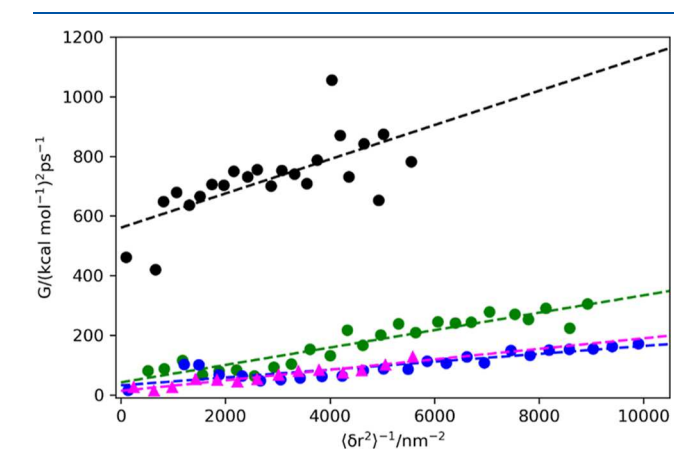


Figure 5. G vs $\langle \delta r^2 \rangle^{-1}$ for polar (blue) and charged contacts (green and black). A linear fit to the data for the polar contacts is plotted with the data (dashed line). The dashed magenta line is the linear fit to polar contacts of the helices of HP36 (ref 54). Charged contacts in green are Tyr117-Asp170 and Arg199-Asp265 and black are Asp194-Arg199 and Asp36-Arg46. Linear fits in the corresponding colors are shown.

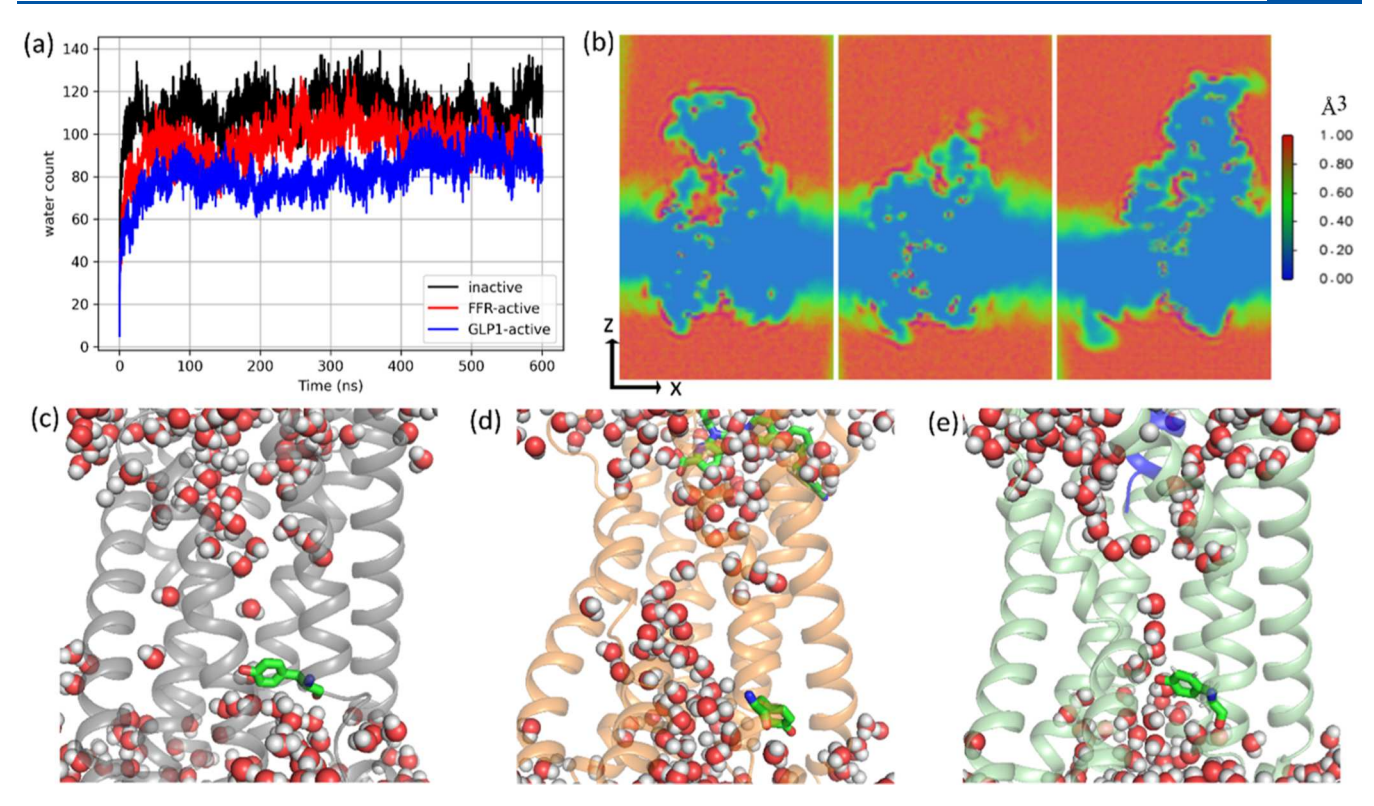


Figure 6. (a) Water count inside the transmembrane region. (b) Water density maps computed from 500 to 600 ns. From left to right: inactive, FFR-active, and GFP1-active states. The probability density of water is calculated for each 1 Å^3 grid of the simulation box, which is plotted along the x-z plane as shown in the sidebar and a 1 Å-thick slice along y-axis through the ligand binding region. Bottom row: location of TW at 600 ns. (c) Inactive, (d) FFR-active, and (e) GLP1-active states. The Tyr374 of the HETxmotif is shown, which regulates the water flow inside the transmembrane region.

trendline, which can be fit to (also blue) $G=0.014\langle\delta r^2\rangle^{-1}+32$ with an R^2 value of 0.87. This can be compared to the linear fit to all the data (Figure S4), which yields $G=0.014\langle\delta r^2\rangle^{-1}+22$, and thus, the same slope as the binned data. Since most of these contacts lie at the edge of a helix, it is interesting to compare with earlier results for helices. We have thus included in Figure 5 a fit to the corresponding data obtained for the helices of the villin headpiece subdomain HP36 (magenta) (ref 54), which essentially overlap the data for GLP-1R, suggesting a universality for the proportionality of the rate of energy transfer across polar contacts of helices and fluctuations in the length of the contact.

It is noteworthy that all polar contacts of GLP-1R fall on the same trendline. While most of the contacts lie at the edge of helices, the non-helical contacts may be of more practical interest. The rate of energy transfer across non-covalently bonded contacts contributes far more to the overall rate of energy transfer between residues when the residues are more distant in sequence, as observed, for example, in time-resolved Raman experiments of myoglobin.²⁹ It is therefore significant that all polar contacts of GLP-1R exhibit the same proportionality, not only the helical contacts.

We further examine the relationship of *G* with inverse variance for intact hydrogen bonds between charged groups, which include Asp36-Arg46, Tyr117-Asp170, Asp194-Arg199, and Arg199-Asp265, where Asp36-Arg46 is found for all three states. All data are plotted in Figure S5, where the contacts appear to fall into two groups. We plot the smoothed data for clarity in Figure 5 (smoothing detailed in Section 2), where the two groups appear as green and black. A linear fit to the green

data, corresponding to Tyr117-Asp170 and Arg199-Asp265, yields $G=0.029\langle\delta r^2\rangle^{-1}+42$ with an R^2 of 0.93. This is very close to the linear fit, $G=0.032\langle\delta r^2\rangle^{-1}+27$, to all the data (Figure S5). A linear fit to the black data, corresponding to Asp194-Arg199 and Asp36-Arg46, yields $G=0.057\langle\delta r^2\rangle^{-1}+560.5$ with an R^2 of 0.7. The complete set of data points are plotted in Figure S5, where a linear fit yields $G=0.046\langle\delta r^2\rangle^{-1}+600.2$. This fit does not compare well to the fit to the binned data. A linear fit to the data for these charged contacts is less convincing.

For the charged contacts Tyr117-Asp170 and Arg199-Asp265 (green), the inverse proportionality between the rate of energy transfer across the contact and the variance in the length of the contact holds up well. For these contacts, the change in entropy associated with change in dynamics of the contact upon activation can be confidently estimated using the Δ EEN. This is not so surprising for Tyr117-Asp170, since the contact is formed by a single O- from Asp170 and the OH group of the side chain of Tyr117, thereby forming a polar contact for which the proportionality is expected. However, Arg199-Asp265 is more surprising since Asp-Arg contacts often do not conform to the scaling relation between rates of energy transfer and equilibrium contact fluctuations. 53,55 Indeed, for Asp194-Arg199 and Asp36-Arg46, this relation holds up less well. However, the Arg199-Asp265 contact is formed between O on the backbone and an H⁺ on the side chain, rather than side chain-side chain interactions, which involve multiple O-H+ interactions, as is usually the case for the Asp-Arg interactions studied in the past.

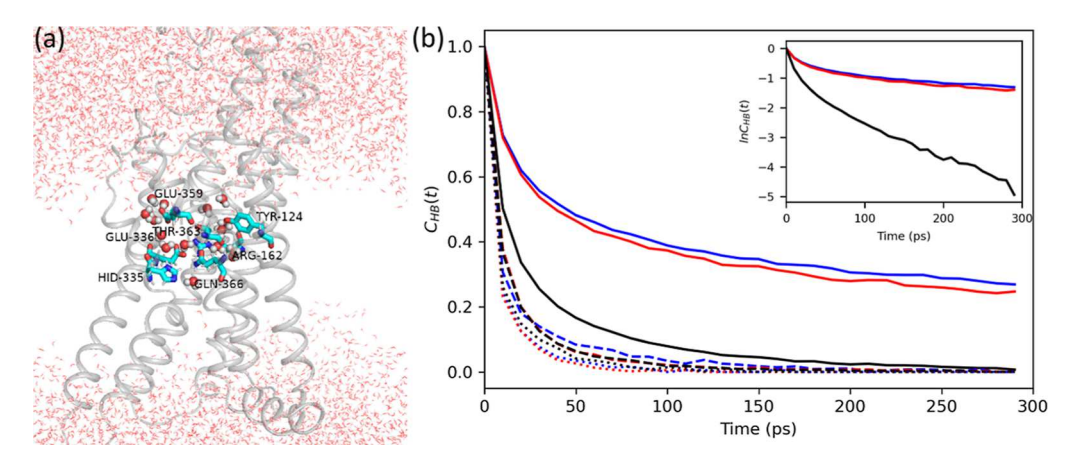


Figure 7. (a) Location of the residues of the central polar network (cyan) and TW (spheres) within 3 Å of the central polar network. The remaining water molecules of the system are shown using lines. (b) Hydrogen bond correlation functions, $C_{HB}(t)$, of protein-water of the GLP-1R in all three states. Blue indicates the GLP1-active state, red indicates the FFR-active state, and black indicates the inactive state. Solid curves correspond to hydrogen bonds between residues of the center polar region and TW. Dashed curves correspond to hydrogen bonds between water and residues of intracellular loops. The dotted curves correspond to hydrogen bonds between water and the extracellular domain. The inset is a semi-log plot for the protein-TW hydrogen bonds involving the central polar network.

We now estimate change in entropy, $\Delta S = S_2 - S_1$, upon activation due to change in G, given by eq 1. This estimate follows from the proportionality between G and $\langle \delta r^2 \rangle^{-1}$. We see in Figure 5 that this relation holds well for the polar contacts plotted in Figure 5 as well as for some but not all the charged contacts plotted there. For this reason, we consider only the polar contacts represented by the blue data points in Figure 5. The data for the active and inactive states are plotted in Figure S4 and the average values of G for each state are listed in Table S1. For four of the seven contacts, the larger average value of G is for the inactive state, and for the other three, it is the active state. The range of ΔS is -4.6 to 3.1 J mol⁻¹ K⁻¹, and the average change in entropy, positive or negative, is about 2.6 J mol⁻¹ K⁻¹, or a contribution of 0.8 kJ mol⁻¹ to the free energy change for each contact at 300 K. The sign of the entropy difference depends on the contact. We note that for two nearby contacts, the change in dynamics may be correlated, so that the entropy change associated with each contact would not be simply additive. The location of the seven contacts considered here, shown in Figure S6, ranges from the cytoplasmic region toward the ligand binding region, but correlations cannot be ruled out.

The illustration provided here for these contacts indicates that measurements of changes in the rate of energy transfer across a contact with activation can reveal changes in entropy associated with the dynamics of the contact and can thereby provide a local probe of dynamic and entropic contributions to activation. These changes appear to be often in the range 1-5 J mol $^{-1}$ K $^{-1}$, making a significant contribution to the free energy of activation. We note that the ratio G_1/G_2 in eq 1 can be quite large (or small) even if the difference between G_1 and G_2 is not great. This means that nonpolar contacts, for which G_1 and G_2 are usually small so that their difference is small, ⁵⁴ may exhibit large change in dynamics and associated entropy upon activation, which could be detected by measurement of rates of energy transfer across the contact in different functional states.

3.3. TW Dynamics. We have seen that water contributes to energy transport through GLP-1R. We now consider TW dynamics to explore some of the functional roles of water and water-mediated interactions, in particular, toward signaling and

activation. Water near protein surfaces is dynamically and thermodynamically distinct from bulk water, particularly in the protein interior. For the three states of GLP-1R, we indicate the number of TW water during the simulation and the location of the TW at 600 ns in Figure 6.

The total number of TW found in the MD simulations is plotted in Figure 6a. The TW includes water flowing between the transmembrane region and both the extracellular and cytoplasmic sides of the receptor. On the extracellular side, water can penetrate into the ligand binding region of the inactive state, while it is blocked from this region due to the presence of ligands in the active states. This contributes to the overall greater number of TW in the inactive state. There are also some differences in the passage of water molecules from the extracellular side in the active states. In the FFR-active state, TWs have penetrated from the vicinity of the ligand, and in the GLP1-active state, they are coming from the vicinity of the peptide ligand, which appears to replace water molecules and occupy a larger cavity of the ligand-binding pocket.

The larger number of TW in the inactive state due to access to the ligand binding region can be seen when plotting the water density in the transmembrane region. In Figure 6b, we plot a density map, computed from the final 100 ns of the MD simulations and calculated for three-dimensional grids of size 1.0 $Å^3$. The image shows a slice 1 Å thick (along the y-axis in the figure) through the middle of the protein that includes the ligand binding pocket. The colors represent an average of the water density in each cell along the xz. The diverse structure of the protein in the extracellular domain for the three states is visible in blue in the upper part of the figure. We also see in Figure 6b a relatively high density of water in the ligandbinding pocket of the inactive state when compared to the two active states, which helps to explain why overall there is more TW in the inactive state (Figure 6a). A similar trend has been found previously for another GPCR.6

There are also other features suggested by the density plot, with some differences in the number of water molecules toward the center of the transmembrane region. Those are seen in Figure 6c-e, for the inactive, FFR-active, and GLP1-active states, respectively. The entire transmembrane region is shown in each case. We see for the FFR-active state more TW

in the middle of the transmembrane region. The water clusters deeper inside the protein are seen to be correlated with the gate orientation, in which Tyr374, which belongs to the HETx motif, blocks the water from the cytoplasmic side in the inactive and GLP1-active state. In the inactive and GLP1-active state, Tyr374 is oriented toward TM6, while in the FFR-active state, the orientation is almost opposite. To confirm the orientation of Tyr374 throughout the simulations, we performed a clustering analysis of Tyr374 in all three states. A total of 10,000 structures were taken from the final 100 ns simulations with a neighbor RMSD cutoff of 0.2 nm. Tyr374 appears in a single cluster, as seen in Figure S7.

The central polar network inside the transmembrane region has been reported to be particularly important to stabilization of the active state. Residues of the central polar network, shown in Figures 1 and 7, are conserved residues in class B GPCRs. Results of previous MD simulations of two active states of GLP-1R indicate long-lived water structures in this region that facilitate stabilization of the active state. It is therefore worthwhile comparing dynamics of water molecules in contact with the central polar network in the inactive and the active states. We do this by computing the correlation function for hydrogen bonds, $C_{\rm HB}(t)$, between water and residues of the central polar network, which corresponds to the probability that such a hydrogen bond found at some time is found again a time, t, later.

We plot $C_{\rm HB}(t)$ for hydrogen bonds between water molecules and the central polar network in Figure 7. We find that protein-TW hydrogen bonds for the active states relax far more slowly than for the inactive state. Indeed, protein-TW hydrogen bond dynamics for the inactive state are comparable to the relaxation dynamics of water—protein hydrogen bonds outside the transmembrane region, also plotted in Figure 7. For the latter, we find no significant difference in the hydrogen bond dynamics for inactive and active states. However, the dynamics is slightly slower for the intracellular region compared to the extracellular region due to a larger fraction of charged groups in contact with water for the former. In the intracellular region, the ratio of charged to total residues is 0.35, while it is 0.22 in the extracellular domain. The ratio is 0.30 in the central polar network of the transmembrane region.

To estimate time constants for the relaxation of protein—water hydrogen bonds for the central polar network region, we simply consider the time for $C_{\rm HB}(t)$ to reach ${\rm e}^{-1}$ (inset to Figure 7b), yielding time constants for the GLP1-active, FFR-active, and inactive states of 114.8, 98.2, and 15.1 ps, respectively. The slow relaxation of TW in the active states facilitates their stabilization and is consistent with the role of water-central polar network interactions, which have been reported to stabilize the active state of GLP-1R. ¹⁶

4. CONCLUSIONS

We have carried out MD simulations of the inactive and two active states of GLP-1R, a class B GPCR, one member of a family of receptors for which structures have only recently become available. For the two active states, one activated by a peptide ligand and the other by a small molecule agonist, the overall transmembrane (TM) structure is similar, though there are notable differences in some side-chain orientations and larger structural and dynamic differences in the extracellular domain (ECD). In the transmembrane central polar network region, we find strikingly slower water dynamics for the active states compared to the inactive state. This property is

consistent with relatively long-lived water structures in this region for active states studied in earlier work, ¹⁶ consistent with TW stabilizing the active states, a property also seen previously for a class A, rhodopsin-like GPCR.⁶ Despite different motifs found for class A and class B GPCRs, water appears to play a similar role in activation.

We have also examined energy transport in the inactive and two active states of GLP-1R, by computing energy exchange networks (EENs). Earlier calculations of EENs have shown how changes in the EENs with ligand binding reveal structural changes involved in activation, 41 including a study of the eta_2 adrenergic receptor, a rhodopsin-like GPCR. 42,76 Similarly, for GLP-1R, significant changes in the EENs are found among residues belonging to motifs, where structural changes important for activation occur. We have also examined how changes in the EEN upon activation reveal dynamic differences in the inactive and active states. Important changes in the EENs also occur where non-covalent contacts remain intact during activation, but dynamics of the contact change. For almost all of these contacts, we find an inverse proportionality between the rate of energy transfer across the contact and variance in the length of the contact. The change in entropy associated with changes in dynamics of the contact due to activation can thereby be estimated from information about the change in the rate of energy transfer across the contact, a property that can be measured by time-resolved IR and time-resolved Raman spectroscopy. ^{29,77–83} For all the contacts examined here where dynamic but not structural changes contribute most to the change in the EEN, we find associated entropy changes of magnitude 1-5 J mol⁻¹ K⁻¹, contributing significantly to the free energy of activation. We have also found TW to make important contributions to the EENs of GLP-1R.

It would be of interest to study other class B GPCRs and members of the B1 subfamily by MD simulations to better understand the activation mechanism and allosteric regulation. Many structures of the 15 members of this subfamily, which includes GLP-1R, are now known,84 though some antagonistbound inactive and apo inactive structures remain unknown. It is noteworthy that for the known class B1 structures, the main differences among inactive or active states are the structures of the ECD; the TM region appears similar for members of this subfamily, as was the case for the two active states of GLP-1R studied here despite very different ligands. We therefore expect similar trends to those we found for GLP-1R to hold for other class B1 GPCRs. Nevertheless, more detailed studies are needed, including the role of water, to identify common and unique structural features important for GPCR function and future receptor design and allosteric drug development.⁸⁵

ASSOCIATED CONTENT

Supporting Information

The Supporting Information is available free of charge at https://pubs.acs.org/doi/10.1021/acs.jpcb.2c03960.

EEN; complete G versus $\langle \delta r^2 \rangle^{-1}$ data; clustering analysis; water bridges; RMSF and RMSD; and tables of residue—residue and residue-TW values of G and estimates of entropy change (PDF)

AUTHOR INFORMATION

Corresponding Author

David M. Leitner – Department of Chemistry, University of Nevada, Reno, Nevada 89557, United States; o orcid.org/0000-0002-3105-818X; Email: dml@unr.edu

Author

Humanath Poudel – Department of Chemistry, University of Nevada, Reno, Nevada 89557, United States

Complete contact information is available at: https://pubs.acs.org/10.1021/acs.jpcb.2c03960

Notes

The authors declare no competing financial interest.

ACKNOWLEDGMENTS

Support from NSF grant CHE-1854271 is gratefully acknowledged. The authors are grateful to the Cyberinfrastructure Team in the Office of Information Technology at UNR for access to the Pronghorn HPC cluster, with allocation supported by UNR Student Technology Fees.

REFERENCES

- (1) Burg, J. S.; Ingram, J. R.; Venkatakrishnan, A. J.; Jude, K. M.; Dukkipati, A.; Feinberg, E. N.; Angelini, A.; Waghray, D.; Dror, R. O.; Ploegh, H.; et al. Structural Basis for Chemokine Recognition and Activation of a Viral G Protein-Coupled Receptor. *Science* **2015**, 347, 1113–1117.
- (2) Trzaskowski, B.; Latek, D.; Yuan, S.; Ghoshdastider, U.; Debinski, A.; Filipek, S. Action of Molecular Switches in GPCRs Theoretical and Experimental Studies. *Curr. Med. Chem.* **2012**, *19*, 1090–1109.
- (3) Latorraca, N. R.; Venkatakrishnan, A. J.; Dror, R. O. GPCR Dynamics: Structures in Motion. *Chem. Rev.* **2017**, *117*, 139–155.
- (4) Venkatakrishnan, A. J.; Ma, A. K.; Fonseca, R.; Latorraca, N. R.; Kelly, B.; Betz, R. M.; Asawa, C.; Kobilka, B. K.; Dror, R. O. Diverse Gpcrs Exhibit Conserved Water Networks for Stabilization and Activation. *Proc. Natl. Acad. Sci.* **2019**, *116*, 3288–3293.
- (5) Lee, Y.; Choi, S.; Hyeon, C. Mapping the intramolecular signal transduction of G-protein coupled receptors. *Proteins: Struct., Funct., Bioinf.* **2014**, 82, 727–743.
- (6) Lee, Y.; Kim, S.; Choi, S.; Hyeon, C. Ultraslow Water-Mediated Transmembrane Interactions Regulate the Activation of A2a Adenosine Receptor. *Biophys. J.* **2016**, *111*, 1180–1191.
- (7) Huang, S. K.; Pandey, A.; Tran, D. P.; Villanueva, N. L.; Kitao, A.; Sunahara, R. K.; Sljoka, A.; Prosser, R. S. Delineating the Conformational Landscape of the Adenosine A2a Receptor During G Protein Coupling. *Cell* **2021**, *184*, 1884–1894.
- (8) Venkatakrishnan, A. J.; Deupi, X.; Lebon, G.; Tate, C. G.; Schertler, G. F.; Babu, M. M. Molecular Signatures of G Protein Coupled Receptors. *Nature* **2013**, *494*, 185–194.
- (9) Hollenstein, K.; de Graaf, C.; Bortolato, A.; Wang, M.-W.; Marshall, F. H.; Stevens, R. C. Insights into the Structure of Class B GPCRs. *Trends Pharmacol. Sci.* **2014**, *35*, 12–22.
- (10) Wu, F.; Yang, L.; Hang, K.; Laursen, M.; Wu, L.; Han, G. W.; Ren, Q.; Roed, N. K.; Lin, G.; Hanson, M. A.; et al. Full-Length Human GLP-1 Receptor Structure without Orthosteric Ligands. *Nat. Commun.* **2020**, *11*, 1272.
- (11) Krumm, B.; Roth, B. L. A Structural Understanding of Class B GPCR Selectivity and Activation Revealed. *Structure* **2020**, 28, 277–279.
- (12) Liang, Y.-L.; Khoshouei, M.; Radjainia, M.; Zhang, Y.; Glukhova, A.; Tarrasch, J.; Thal, D. M.; Furness, S. G. B.; Christopoulos, G.; Coudrat, T.; et al. Phase-Plate Cryo-Em Structure of a Class B GPCR—G-Protein Complex. *Nature* 2017, 546, 118—123.

- (13) Zhang, Y.; Sun, B.; Feng, D.; Hu, H.; Chu, M.; Qu, Q.; Tarrasch, J. T.; Li, S.; Sun Kobilka, T. S.; Kobilka, B. K.; Skiniotis, G. Cryo-EM Structure of the Activated GLP-1 Receptor in Complex with a G Protein. *Nature* **2017**, *546*, 248–253.
- (14) Song, G.; Yang, D.; Wang, Y.; de Graaf, C.; Zhou, Q.; Jiang, S.; Liu, K.; Cai, X.; Dai, A.; Lin, G.; Liu, D.; Wu, F.; Wu, Y.; Zhao, S.; Ye, L.; Han, G. W.; Lau, J.; Wu, B.; Hanson, M. A.; Liu, Z.-J.; Wang, M.-W.; Stevens, R. C. Human GLP-1 Receptor Transmembrane Domain Structure in Complex with Allosteric Modulators. *Nature* **2017**, *546*, 312–315.
- (15) Zhang, H.; Qiao, A.; Yang, D.; Yang, L.; Dai, A.; de Graaf, C.; Reedtz-Runge, S.; Dharmarajan, V.; Zhang, H.; Han, G. W.; et al. Structure of the Full-Length Glucagon Class B G-Protein-Coupled Receptor. *Nature* **2017**, *546*, 259–264.
- (16) Zhao, P.; Liang, Y.-L.; Belousoff, M. J.; Deganutti, G.; Fletcher, M. M.; Willard, F. S.; Bell, M. G.; Christe, M. E.; Sloop, K. W.; Inoue, A.; et al. Activation of the GLP-1 Receptor by a Non-Peptidic Agonist. *Nature* **2020**, *577*, 432–436.
- (17) Ma, H.; Huang, W.; Wang, X.; Zhao, L.; Jiang, Y.; Liu, F.; Guo, W.; Sun, X.; Zhong, W.; Yuan, D.; et al. Structural Insights into the Activation of GLP-1R by a Small Molecule Agonist. *Cell Res.* **2020**, 30, 1140–1142.
- (18) Mattedi, G.; Acosta-Gutiérrez, S.; Clark, T.; Gervasio, F. L. A combined activation mechanism for the glucagon receptor. *Proc. Natl. Acad. Sci.* **2020**, *117*, 15414–15422.
- (19) Yuan, S.; Vogel, H.; Filipek, S. The Role of Water and Sodium Ions in the Activation of the Mu-Opioid Receptor. *Angew. Chem., Int. Ed. Engl.* **2013**, *52*, 10112–10115.
- (20) Bertalan, É.; Lešnik, S.; Bren, U.; Bondar, A. N. Protein-Water Hydrogen-Bond Networks of G Protein-Coupled Receptors: Graph-Based Analyses of Static Structures and Molecular Dynamics. *J. Struct. Biol.* **2020**, *212*, 107634.
- (21) Yuan, S.; Filipek, S.; Palczewski, K.; Vogel, H. Activation of G-Protein-Coupled Receptors Correlates with the Formation of a Continuous Internal Water Pathway. *Nat. Commun.* **2014**, *5*, 4733.
- (22) Sun, X. Q.; Ågren, H.; Tu, Y. Q. Functional Water Molecules in Rhodopsin Activation. *J. Phys. Chem. B* **2014**, *118*, 10863–10873.
- (23) Bortolato, A.; Doré, A. S.; Hollenstein, K.; Tehan, B. G.; Mason, J. S.; Marshall, F. H. Structure of Class B GPCRs: New Horizons for Drug Discovery. *Br. J. Pharmacol.* **2014**, *171*, 3132–3145.
- (24) Graaf, C.; Donnelly, D.; Wootten, D.; Lau, J.; Sexton, P. M.; Miller, L. J.; Ahn, J. M.; Liao, J.; Fletcher, M. M.; Yang, D.; et al. Glucagon-Like Peptide-1 and Its Class B G Protein-Coupled Receptors: A Long March to Therapeutic Successes. *Pharmacol. Rev.* 2016, 68, 954–1013.
- (25) Nauck, M. A.; Meier, J. J. Management of Endocrine Disease: Are all GLP-1 agonists equal in the treatment of type 2 diabetes? *Eur. J. Endocrinol.* **2019**, *181*, R211–R234.
- (26) Malik, F.; Li, Z. Non-Peptide Agonists and Positive Allosteric Modulators of Glucagon-Like Peptide-1 Receptors: Alternative Approaches for Treatment of Type 2 Diabetes. *Br. J. Pharmacol.* **2021**, *179*, 511–525.
- (27) Zhang, X.; Belousoff, M. J.; Zhao, P.; Kooistra, A. J.; Truong, T. T.; Ang, S. Y.; Underwood, C. R.; Egebjerg, T.; Šenel, P.; Stewart, G. D.; et al. Differential GLP-1R Binding and Activation by Peptide and Non-Peptide Agonists. *Mol. Cell* **2020**, *80*, 485–500.
- (28) Leitner, D. M. Energy Flow in Proteins. *Annu. Rev. Phys. Chem.* **2008**, *59*, 233–259.
- (29) Fujii, N.; Mizuno, M.; Ishikawa, H.; Mizutani, Y. Observing Vibrational Energy Flow in a Protein with the Spatial Resolution of a Single Amino Acid Residue. *J. Phys. Chem. Lett.* **2014**, *5*, 3269–3273.
- (30) Leitner, D. M.; Straub, J. E. Proteins: Energy, Heat and Signal Flow; CRC Press, Taylor & Francis Group: Boca Raton, FL, 2010.
- (31) Ishikura, T.; Yamato, T. Energy Transfer Pathways Relevant for Long-Range Intramolecular Signaling of Photosensory Protein Revealed by Microscopic Energy Conductivity Analysis. *Chem. Phys. Lett.* **2006**, 432, 533–537.

- (32) Leitner, D. M.; Yamato, T.Mapping Energy Transport Networks in Proteins. In *Reviews in Computational Chemistry*; Parrill, A. L., Lipkowitz, K. B., Eds.; John Wiley & Sons, Inc., 2018; Vol. 31, pp 63–113.
- (33) Leitner, D. M.; Yamato, T. Recent Developments in the Computational Study of Protein Structural and Vibrational Energy Dynamics. *Biophys. Rev.* **2020**, *12*, 317–322.
- (34) Xu, Y.; Leitner, D. M. Vibrational Energy Flow through the Green Fluorescent Protein-Water Interface: Communication Maps and Thermal Boundary Conductance. *J. Phys. Chem. B* **2014**, *118*, 7818–7826.
- (35) Buchenberg, S.; Leitner, D. M.; Stock, G. Scaling Rules for Vibrational Energy Transport in Proteins. *J. Phys. Chem. Lett.* **2016**, 7, 25–30.
- (36) Gulzar, A.; Valiño Borau, L.; Buchenberg, S.; Wolf, S.; Stock, G. Energy Transport Pathways in Proteins: A Nonequilibrium Molecular Dynamics Simulation Study. *J. Chem. Theory Comput.* **2019**, *15*, 5750–5757.
- (37) Leitner, D. M.; Buchenberg, S.; Brettel, P.; Stock, G. Vibrational Energy Flow in the Villin Headpiece Subdomain: Master Equation Simulations. *J. Chem. Phys.* **2015**, *142*, 075101.
- (38) Valiño Borau, L.; Gulzar, A.; Stock, G. Master Equation Model to Preduct Energy Transport Pathways in Proteins. *J. Chem. Phys.* **2020**, *152*, 045103.
- (39) Nagaoka, M.; Yu, I.; Takayanagi, M.Energy Flow Analysis in Proteins Via Ensemble Molecular Dynamics Simulations: Time-Resolved Vibrational Analysis and Surficial Kirkwood-Buff Theory. In *Proteins: Energy, Heat and Signal Flow*; Leitner, D. M., Straub, J. E., Eds.; Taylor & Francis Group, CRC Press: Boca Raton, 2010; pp 169–196.
- (40) Takayanagi, M.; Okumura, H.; Nagaoka, M. Anisotropic Structural Relaxation and Its Correlation with the Excess Energy Diffusion in the Incipient Process of Photodissociated Mbco: High-Resolution Analysis Via Ensemble Perturbation Method. *J. Phys. Chem. B* **2007**, *111*, 864–869.
- (41) Ota, K.; Yamato, T. Energy Exchange Network Model Demonstrates Protein Allosteric Transition: An Application to an Oxygen Sensor Protein. *J. Phys. Chem. B* **2019**, *123*, 768–775.
- (42) Poudel, H.; Leitner, D. M. Activation-Induced Reorganization of Energy Transport Networks in the B2adrenergic Receptor. *J. Phys. Chem. B* **2021**, *125*, 6522–6531.
- (43) Ishikura, T.; Iwata, Y.; Hatano, T.; Yamato, T. Energy Exchange Network of Inter-Residue Interactions within a Thermally Fluctuating Protein: A Computational Study. *J. Comput. Chem.* **2015**, *36*, 1709–1718.
- (44) Yamato, T.; Wang, T.; Sugiura, W.; Laprévote, O.; Katagiri, T. Computational Study on the Thermal Conductivity of a Protein. *J. Phys. Chem. B* **2022**, *126*, 3029–3036.
- (45) Fiser, A.; Sali, A. Modloop: Automated Modeling of Loops in Protein Structures. *Bioinformatics* **2003**, *19*, 2500–2501.
- (46) Allouche, A.-R. Software News and Updates Gabedit a Graphical User Interface for Computational Chemistry Softwares. *J. Comput. Chem.* **2011**, 32, 174–182.
- (47) Dickson, C. J.; Madej, B. D.; Skjevik, Å. A.; Betz, R. M.; Teigen, K.; Gould, I. R.; Walker, R. C. Lipid14: The Amber Lipid Force Field. *J. Chem. Theory Comput.* **2014**, *10*, 865–879.
- (48) Maier, J. A.; Martinez, C.; Kasavajhala, K.; Wickstrom, L.; Hauser, K. E.; Simmerling, C. Ff14sb: Improving the Accuracy of Protein Side Chain and Backbone Parameters from Ff99sb. J. Chem. Theory Comput. 2015, 11, 3696–3713.
- (49) Berendsen, H. J. C.; Postma, J. P. M.; van Gunsteren, W. F.; DiNola, A.; Haak, J. R. Molecular Dynamics with Coupling to an External Bath. *J. Chem. Phys.* **1984**, *81*, 3684–3690.
- (50) Darden, T.; York, D.; Pedersen, L. Particle Mesh Ewald: An N Log(N) Method for Ewald Sums in Large Systems. *J. Chem. Phys.* **1993**, *98*, 10089–10092.
- (51) Yamato, T.Energy Flow Pathways in Photoreceptor Proteins. In Proteins: Energy, Heat and Signal Flow; Leitner, D. M., Straub, J. E.,

- Eds.; CRC Press, Taylor and Francis Group: Boca Raton, 2010; pp 129-147.
- (52) Leitner, D. M.; Pandey, H. D.; Reid, K. M. Energy Transport across Interfaces in Biomolecular Systems. *J. Phys. Chem. B* **2019**, *123*, 9507–9524
- (53) Reid, K. M.; Yamato, T.; Leitner, D. M. Scaling of Rates of Vibrational Energy Transfer in Proteins with Equilibrium Dynamics and Entropy. *J. Phys. Chem. B* **2018**, *122*, 9331–9339.
- (54) Poudel, H.; Reid, K. M.; Yamato, T.; Leitner, D. M. Energy Transfer across Nonpolar and Polar Contacts in Proteins: Role of Contact Fluctuations. *J. Phys. Chem. B* **2020**, 124, 9852–9861.
- (55) Reid, K. M.; Yamato, T.; Leitner, D. M. Variation of Energy Transfer Rates across Protein—Water Contacts with Equilibrium Structural Fluctuations of a Homodimeric Hemoglobin. *J. Phys. Chem. B* **2020**, *124*, 1148—1159.
- (56) Ebbinghaus, S.; Kim, S. J.; Heyden, M.; Yu, X.; Heugen, U.; Gruebele, M.; Leitner, D. M.; Havenith, M. An Extended Dynamical Hydration Shell around Proteins. *Proc. Natl. Acad. Sci.* **2007**, *104*, 20749–20752.
- (57) Tarek, M.; Tobias, D. J. Role of Protein-Water Hydrogen Bond Dynamics in the Protein Dynamical Transition. *Phys. Rev. Lett.* **2002**, 88, 138101–138114.
- (58) Reid, K. M.; Singh, A. K.; Bikash, C. R.; Wei, J.; Tal-Gan, Y.; Vinh, N. Q.; Leitner, D. M. The Origin and Impact of Bound Water around Intrinsically Disordered Proteins. *Biophys. J.* **2022**, *121*, 540–551
- (59) Bagchi, B. Water Dynamics in the Hydration Layer around Proteins and Miscelles. *Chem. Rev.* **2005**, *105*, 3197–3219.
- (60) Gnanasekaran, R.; Agbo, J. K.; Leitner, D. M. Communication Maps Computed for Homodimeric Hemoglobin: Computational Study of Water-Mediated Energy Transport in Proteins. *J. Chem. Phys.* **2011**, *135*, 065103.
- (61) Bozovic, O.; Zanobini, C.; Gulzar, A.; Jankovic, B.; Buhrke, D.; Post, M.; Wolf, S.; Stock, G.; Hamm, P. Real-Time Observation of Ligand-Induced Allosteric Transitions in a Pdz Domain. *Proc. Natl. Acad. Sci.* **2020**, *117*, 26031–26039.
- (62) Motlagh, H. N.; Wrabl, J. O.; Li, J.; Hilser, V. J. The Ensemble Nature of Allostery. *Nature* **2014**, *508*, 331–339.
- (63) Saavedra, H. G.; Wrabl, J. O.; Anderson, J. A.; Li, J.; Hilser, V. J. Dynamic Allostery Can Drive Cold Adaptation in Enzymes. *Nature* **2018**, 558, 324–328.
- (64) Leitner, D. M.; Hyeon, C.; Reid, K. M. Water-Mediated Biomolecular Dynamics and Allostery. *J. Chem. Phys.* **2020**, *152*, 240901.
- (65) Cooper, A.; Dryden, D. T. F. Allostery without Conformational Change: A Plausible Model. *Eur. Biophys. J.* **1984**, *11*, 103–109.
- (66) Cui, Q.; Karplus, M. Allostery and Cooperativity Revisited. *Protein Sci.* **2008**, *17*, 1295–1307.
- (67) Reid, K. M.; Yu, X.; Leitner, D. M. Change in Vibrational Entropy with Change in Protein Volume Estimated with Mode Grüneisen Parameters. *J. Chem. Phys.* **2021**, *154*, 055012.
- (68) Popovych, N.; Sun, S.; Ebright, R. H.; Kalodimos, C. G. Dynamically Driven Protein Allostery. *Nat. Struct. Mol. Biol.* **2006**, *13*, 831–838.
- (69) Leander, M.; Yuan, Y.; Meger, A.; Cui, Q.; Raman, S. Functional Plasticity and Evolutionary Adaptation of Allosteric Regulation. *Proc. Natl. Acad. Sci.* **2020**, *117*, 25445–25454.
- (70) Yu, X.; Park, J.; Leitner, D. M. Thermodynamics of Protein Hydration Computed by Molecular Dynamics and Normal Modes. *J. Phys. Chem. B* **2003**, *107*, 12820–12828.
- (71) Gnanasekaran, R.; Xu, Y.; Leitner, D. M. Dynamics of Water Clusters Confined in Proteins: A Molecular Dynamics Simulation Study of Interfacial Waters in a Dimeric Hemoglobin. *J. Phys. Chem. B* **2010**, *114*, 16989–16996.
- (72) Heyden, M. Heterogeneity of Water Structure and Dynamics at the Protein-Water Interface. *J. Chem. Phys.* **2019**, *150*, 094701.
- (73) Heyden, M.; Tobias, D. J.; Matyushov, D. V. Terahertz Absorption of Dilute Aqueous Solutions. *J. Chem. Phys.* **2012**, *137*, 235103.

- (74) Martin, D. R.; Matyushov, D. V. Terahertz Absorption of Lysozyme in Solution. J. Chem. Phys. 2017, 147, 084502.
- (75) Leitner, D. M.; Gruebele, M.; Havenith, M. Solvation Dynamics of Biomolecules: Modeling and Terahertz Experiments. HFSP J. 2008,
- (76) Di Paola, L.; Poudel, H.; Parise, M.; Giuliani, A.; Leitner, D. M. A Statistical Journey through the Topological Determinants of the B2 Adrenergic Receptor Dynamics. Entropy 2022, 24, 998.
- (77) Fujii, N.; Mizuno, M.; Mizutani, Y. Direct Observation of Vibrational Energy Flow in Cytochrome C. J. Phys. Chem. B 2011, 115, 13057-13064.
- (78) Kondoh, M.; Mizuno, M.; Mizutani, Y. Importance of Atomic Contacts in Vibrational Energy Flow in Proteins. J. Phys. Chem. Lett. **2016**, 7, 1950-1954.
- (79) Mizutani, Y. Time-Resolved Resonance Raman Spectroscopy and Application to Studies on Ultrafast Protein Dynamics. Bull. Chem. Soc. Jpn. 2017, 90, 1344-1371.
- (80) Yamashita, S.; Mizuno, M.; Tran, D. P.; Dokainish, H.; Kitao, A.; Mizutani, Y. Vibrational Energy Transfer from Heme through Atomic Contacts in Proteins. J. Phys. Chem. B 2018, 122, 5877-5884.
- (81) Baumann, T.; Hauf, M.; Schildhauer, F.; Eberl, K. B.; Durkin, P. M.; Deniz, E.; Löffler, J. G.; Acevedo-Rocha, C. G.; Jaric, J.; Martins, B. M.; et al. Site-Resolved Observation of Vibrational Energy Transfer Using a Genetically Encoded Ultrafast Heater. Angew. Chem. 2019, 58, 2899-2903.
- (82) Deniz, E.; et al. Through Bonds or Contacts? Mapping Protein Vibrational Energy Transfer Using Non-Canonical Amino Acids. Nat. Commun. 2021, 12, 3284.
- (83) Yamashita, S.; Mizuno, M.; Mizutani, Y. High Suitability of Tryptophan Residues as a Spectroscopic Thermometer for Local Temperature in Proteins under Nonequilibrium Conditions. J. Chem. Phys. 2022, 156, 075101.
- (84) Cong, Z.; Liang, Y.-L.; Zhou, Q.; Darbalaei, S.; Zhao, F.; Feng, W.; Zhao, L.; Xu, H. E.; Yang, D.; Wang, M.-W. Structural Perspective of Class B1 GPCR Signaling. Trends Pharmacol. Sci. 2022, 43, 321-334.
- (85) Chen, K.-Y. M.; Keri, D.; Barth, P. Computational Design of G Protein-Coupled Receptor Allosteric Signal Transductions. Nat. Chem. Biol. 2020, 16, 77-86.

□ Recommended by ACS

Thermodynamics and Free Energy Landscape of BAR-**Domain Dimerization from Molecular Simulations**

Adip Jhaveri, Margaret E. Johnson, et al.

APRII 07 2021

THE JOURNAL OF PHYSICAL CHEMISTRY B

READ 2

Conformational Analysis of the Loop-to-Helix Transition of the α-Helix3 Plastic Region in the N-Terminal Domain of Human Hsp90α by a Computational Biochemistry Approach

Keigo Gohda.

OCTOBER 24, 2022

JOURNAL OF CHEMICAL INFORMATION AND MODELING

READ **C**

Identification of an α-MoRF in the Intrinsically Disordered **Region of the Escargot Transcription Factor**

Teresa Hernández-Segura and Nina Pastor

JULY 17, 2020

ACS OMEGA

RFAD 17

Analytical Approaches for Deriving Friction Coefficients for Selected α-Helical Peptides Based Entirely on Molecular **Dynamics Simulations**

Aleksandra Wosztyl, Robert Szoszkiewicz, et al.

OCTOBER 27, 2022

THE JOURNAL OF PHYSICAL CHEMISTRY B

RFAD 🗹

Get More Suggestions >